International Symposium On Trial Embankments On Malaysian Marine Clays
November 6-8, 1989, Kuala Lumpur

SOME OBSERVATIONS ON THE PERFORMANCES OF THE SCHEMES

C. T. TOH Dr. C. T. Toh Sdn. Bhd., Kuala Lumpur, Malaysia
S. K. CHEE Dr. C. T. Toh Sdn. Bhd., Kuala Lumpur, Malaysia
R. R. HUDSON Acer Freeman Fox, Kuala Lumpur, Malaysia

1.0 INTRODUCTION

The original intention of the Malaysian Highway Authority when initiating the Trials was to study the possibility of using soil improvement techniques to replace pile embankments on soft ground.

The data collected from the individual embankments when viewed together provides an excellent opportunity to :-

(i) Study the fundamental behaviour of embankments on soft clay;

(ii) Study the behaviour of a pile embankment of the type where the embankment rests on piles with individual pile caps;

(iii) Assess the effectiveness of different techniques of soil improvement by comparing the different schemes with one another as well as the two control embankments.

2.0 INTERFERENCE

Prior to a study of the different schemes it is necessary to establish the degree of interference, if any, between adjoining schemes.

The schemes were arranged to be adjacent to each other because of land constraints and so that in the longer term the area for the trials could be reverted for use as a lay-by. It was also arranged so that adjoining schemes were of similar heights to permit vehicular access. As a consequence of this requirement adjoining schemes were constructed at approximately similar rates. Where instabilities occurred or where significant lateral movement took place with tension cracks appearing, such occurences tended to occur in groups. Examples are :-

(i) Tension cracks and significant lateral movements took place at about the same time for Schemes 3/3 and 3/4 with tension cracks appearing a day earlier at Scheme 3/3 and spreading to Scheme 3/4;

(ii) Instability took place at the same time for Schemes 6/1 and 6/2;

(iii) Significant lateral movements and instability occured at the same time for Schemes 6/4 and 6/5.

It is the opinion of the authors that the individual schemes within each of the above three groups reached states of near instability or instability at about the same time due to similar geometries, similar rates of construction and minimal pore water pressure dissipation within the affected areas. While it is acknowledged that the instability of one scheme did precipitate instability at an adjoining scheme, it is nonetheless felt that the adjoining scheme was near to being unstable in any case.

Fig. 1 illustrates a plot of the movement vectors at RL -2.4m corresponding to the time when the movement toward the adjoining scheme was a maximum. The vectors tend to indicate little evidence of interference between adjoining schemes.

Fig. 2 illustrates the excess pore water pressure, angular rotation (as measured by the inclinometer) and settlement measurements for three adjacent Schemes 6/6. 6/7 and 6/8 all plotted to the same time frame.

Increasing fill thickness from 0.0 to 6.5m at Scheme 6/7 between days 0 and 200 did not cause increased pore pressure at Scheme 6/8, where the fill thickness remained unchanged. The fill thickness at Scheme 6/8 was raised from 5.5m to 8.0m between days 520 and 600 but this did not cause a rotation of the movement vector (from inclinometer measurements) of Scheme 6/7 nor did it cause any increase in differential settlements at Scheme 6/7 (i.e. no change in rate of settlement at S8 compared to S2, which is further away from Scheme 6/8).

All the above indicate relatively little interference between the different schemes.

3.0 EXCESS PORE WATER PRESSURES

3.1 RESPONSE TO LOAD

The excess pore water pressure ($\Delta\mu$) - applied vertical stress ($\Delta\sigma_v$) generally took bi-linear form with the seperation between the two at a fill thickness of about 1.5m. Fig. 3 illustrates the plots at piezometer P4 for some of the schemes.

Figs. 4a and 4b summarize the values of the first and second phase $\Delta\mu/\Delta\sigma_v$ for the centreline piezometers compared to the average line reported by Leroueil and Tavenas (1986). The general range of $\Delta\mu/\Delta\sigma_v$ values are summarized in Table 1 below :-

	1st Phase	2nd Phase
Centreline	0.3 to 0.7	0.7 to 1.0
Edge	0.1 to 0.5	0.5 to 0.9

TABLE 1 General Range of $\Delta\mu/\Delta\sigma_v$

The range of $\Delta\mu/\Delta\sigma_v$ values are similar to those reported by Leroueil and Tavenas (1986) from a study of about 65 embankments world wide.

There appears to be little distinction in $\Delta\mu/\Delta\sigma_v$ for the different soil improvement schemes.

3.2 PORE PRESSURE TIME BEHAVIOUR

For the purpose of comparing the pore pressure dissipation behaviour of the different schemes, the latest available rates of pore pressure change are plotted against depth for all the different schemes in Fig. 5.

As illustrated, appreciable pore pressure dissipation occurred only at Schemes 6/5 and 6/7. All the other schemes showed significantly less pore pressure dissipation with slightly higher rates of dissipation at the top of the clay near to the drainage blanket. Notably the excess pore pressures at those schemes with prebabricated vertical drains (Schemes 3/4, 6/8 and 6/9) exhibited low rates of dissipation, only marginally faster than the schemes without vertical drainage.

While it is apparent from Fig. 5 that it is possible to reduce pore pressures with vacuum and prefabricated vertical drains and sand drains of large diameter as demonstrated at Schemes 6/5 and 6/7, this dissipation of pore pressure was not achieved at Schemes 3/4, 6/8 and 6/9 which used prefabricated vertical drains in a more conventional system.

Instead of pore pressure dissipation, pore pressure stagnation and pore pressure increase under constant vertical stress were observed at several schemes. In some cases the pore pressure increase occured only over a short period and the embankment remained stable thereafter. There were however two cases where the pore pressure increase continued until embankment failure took place.

The details of pore pressure build up under constant applied pressure are summarized in Table 2.

4.0 OVER-CONSOLIDATION RATIOS

Estimates of the over consolidation ratios may be made by constructing ϵ_v - log σ_v' curves where :-

(i) ϵ_v is the vertical strain at piezometer P4 (i.e. at RL -2.4m) computed from data from the Sondex settlement system;

(ii) σ_v is the total stress obtained by use of elastic solutions (Giroud, 1973);

(iii) $\sigma_v' = \sigma_v - \mu$ where μ is the measured pore water pressure.

Scheme	Piezometer	Fill Thickness (m)	Rate of Pore Pressure Increase (mm/day)	Period of Pore Pressure Rise	Comments
3/1	P1	3.78m	4.0	Day 300 to Day 426	Pore pressure subsequently decreased. Embankment remained stable.
	P2		3.7		
	P3		2.0		
	P4		3.8		
	P5		5.0		
	P6		2.7		
3/2	P1	3.90m	1.4	Day 287 to Day 400	Pore pressures subsequently decreased. Embankment remained stable.
	P2		6.6		
	P3		0.9		
	P5		4.8		
6/1	P1	4.68m	25.6	Day 269 to Day 290	Embankment failed at day 290.
	P2		47.6		
	P3		14.3		
	P4		67.1		
	P5		17.1		
	P6		17.1		
6/2	P1	4.10m	12.2	Day 67 to Day 100	Embankment failed at day 100.
	P2		25.8		
	P3		6.7		
6/6	P2	7.25m	3.7	Day 234 to Day 422	Pore pressures subsequently decreased. Embankment remained stable.
	P3		7.4		
6/2	P2	5.73m	4.8	Day 163 to Day 225	P2 showed pore pressure decrease after day 225. Pore pressures remained stagnant at P3 after day 225.
	P3		7.3		

TABLE 2

Typical ϵ_v - log σ_v' curves are given in Figs. 6. The preconsolidation pressures are reached at very low strains. Table 3 presents some of the O.C.R. values of the different schemes where interpretation could reasonably be made.

The field O.C.R. values are comparable with the values from laboratory oedometer tests on undisturbed samples (see the results in Volume 1 from this Proceedings).

Scheme	Field O.C.R.
6/1	1.5
6/2	1.6
6/3	1.6
6/5	2.0
6/6	2.0
6/8	1.7
3/1	1.5
3/2	1.4
3/4	1.4

TABLE 3 Field O.C.R.

5.0 CHANGES IN STRENGTH

Change in strength at time intervals during soil treatment were assessed by vane shear tests and piezocone profiling. The results of such assessment of some schemes are summarized in Figs. 7 and 8.

Appreciable strength gains throughout the full depth of the soft clays were observed only at Schemes 6/5 and 6/7 where appreciable pore water pressure dissipations were recorded.

For the other schemes, strength gain occured only near the sand drainage balnket where some, albeit small, pore pressure dissipation took place. At greater depths, the lack of gain in strength is consistent with the lack of pore pressure dissipation.

It would appear that the ability to achieve gain in strength is directly related to the ability to reduce excess pore pressure and this was only achieved at Schemes 6/5 and 6/7.

6.0 SETTLEMENTS AND LATERAL DISPLACEMENTS

6.1 PLOTS OF MAXIMUM LATERAL DISPLACEMENT VERSUS SETTLEMENT

Fig. 9 illustrates plots of maximum lateral displacement (S_h) versus the settlement (S_v) for all the schemes. Also shown for comparison are those published by Tavenas and Lerouiel (1980).

The S_h - S_v plots for most of the schemes were generally of bilinear form similar to those publised by Tavenas and Leroueil (1980). Lower gradients ($\Delta S_h/\Delta S_v$) were observed at the earlier stages of embankment construction.

The S_h - S_v plots for Schemes 3/3 and 3/4 are distinctly different in that initially higher $\Delta S_h/\Delta S_v$ were observed. This is thought to be due to a significantly high rate of fill placement of about 220mm/day raising the fill thickness to 3.93m over a period of 18 days. Tension cracks were thereafter observed.

6.2 VOLUMETRIC COMPRESSION

The net volume change may be obtained from :-

$$V_c = V_v - V_h$$

where :-

V_v is the vertical volume obtained from integration of the settlement profile of the fill ground interface and ;

V_h is twice the lateral movement volume obtained from integration of the inclinometer profile to account for movements at both edges.

Fig. 10 puts together plots of V_h versus V_v for all the Schemes and those published by Shibata (1987).

The following are observed :-

(i) Significant volumetric compression occured during embankment filling and not a single scheme underwent movement corresponding to an undrained condition;

(ii) Schemes 3/3 and 3/4 where a relatively high rate of fill placement took place exhibited a volume change condition corresponding to a Poisson's ratio of about 0.3;

(iii) Scheme 6/5 also exhibited a Poisson's ratio of 0.3 but with a rate of filling similar to all other schemes;

(iv) Those other schemes showed an initial stage where very significant volume change took place corresponding to a Poisson's ratio of much less than 0.3. A higher component of lateral volume change was observed at a later stage, with Scheme 6/7 being a notable exception.

The V_h versus V_v plot for Scheme 6/6 (control embankment) and Scheme 6/8 were very similar, possibly indicative of the insignificant effects of the prefabricated vertical drains;

(v) Where the gradient of the V_h versus V_v plot shows undrained conditions in the later stages, the embankments were at failure conditions.

6.3 COMPONENTS OF SETTLEMENT

The total measured settlement (S_t) may be regarded as the sum of two components :-

$$S_t = S_c + S_h$$

Where :-

S_c is the component due to volume change, V_c;

and S_h is the component due to lateral movements.

S_c is obtained from V_c by assuming a trapezoidal distribution of S_c while S_h is computed from :-

$$S_h = S_t - S_c$$

The three different components of settlement are computed for all the different schemes and plotted individually in Figs. 11a to 11l and combined in Fig. 12.

With the exception of Scheme 3/3 the S_h components were generally less than 20% of S_t. At Scheme 3/3 the S_h component was approximately 40% of S_t.

6.4 DEGREE OF CONSOLIDATION

The degree of consolidation achieved may be computed from :-

$$U = S_c/S_\infty$$

where :-

$$S_\infty = (Cc/1+eo)\ h\ \log(1 + \Delta P/Po')$$

The values of U were computed for all schemes and plotted in Fig. 13.

Only Scheme 6/7 showed that a significant degree of consolidation had been achieved. This high degree of consolidation is consistent with the degree of pore water pressure dissipation achieved. Unfortunately the inclinometer at Scheme 6/5 stopped functioning at an early stage but the early trend and high rate of pore pressure dissipation indicates that this scheme would also have achieved a significant degree of consolidation.

All the other schemes, which showed minimal pore pressure dissipation, also exhibited a disappointing degree of consolidation. There is little to distinguish the degree of consolidation between the different schemes on treated ground and the control embankments where no treatment was prescribed.

7.0 FAILED EMBANKMENTS

7.1 BACKANALYSIS OF FAILED EMBANKMENTS

Detailed backanalysis of three failed embankments viz. Schemes 3/5 (embankment built to failure), 6/1 and 6/2 was reported by Chee (1991) to determine the embankment and foundation strength.

As it is not possible from Total Stress Analysis alone to backcalculate both the embankment and foundation strengths, Chee (1991) resorted to "a posteriori" type Effective Stress Analysis to first estimate the embankment strength parameter followed by Total Stress Analysis to estimate the foundation strength.

The effective stress analysis was carried out assuming $\emptyset' = 26^0$ for the foundation material (see Vol. 1 of this Proceedings) and analysing a failure surface as interpolated from field surveys of post failure conditions and inclinometer results. Pore water pressures along the failure plane were obtained by linear interpolation of the excess pore water pressure measured at the different piezometer locations. The C', $\emptyset'$ values for the embankment corresponding to a Factor of Safety of 1.0 was deemed to be the correct embankment strength.

Foundation strength was then determined by a Total Stress Analysis with the embankment strength parameters as obtained above. The change in undrained shear strength with depth was similar to that as measured by the field vanes.

The resulting backanalysed parameters were :-

(i) Embankment strength parameters. C' = 14kPa, $\emptyset' = 28^0$ which confirmed the CIU triaxial test results;

(ii) Tension crack length of

$$Z_c = (2C'/\gamma_b)\sqrt{(N\emptyset)}$$

(iii) Vane shear strength correction factors of about 1.0 which is higher than the value of 0.7 to 0.8 derived from Bjerrum's correlation curve.

The method of computation as described above was extended to compute Factors of Safety throughout the construction history. The critical circle at each stage was made to coincide with the level of the maximum shear strain from the inclinometers. The results of the analysis are plotted in Fig. 14 and illustrate a decrease in the Factor of Safety down to a value of 1.0 at the time of failure.

Chee (1991) also concluded that the location of the critical circle from Total Stress Analysis using the Bishop's method coincided reasonably well with the actual failure plane.

7.2 INDICATIONS OF IMPENDING FAILURE

Chee (1991) reported a study of different measurements to try to determine any

discernable trends in pore pressures, lateral movements or location of maximum shear plane which may be indicative of impending failure. Such trends would be useful for controlling embankment construction. The discussions in the above mentioned paper are extended herein below.

7.2.1 SCHEME 6/1

Fig. 15 illustrates plots of fill thickness, pore pressures, lateral movements and locations of the maximum simple shear plane along the inclinometer tube with time. For a fill thickness greater than a relatively low height of about 2.4m, pore pressure stagnation and pore pressure increase under constant embankment thickness were observed. Pore pressure increase under constant applied pressure was most prenounced for the upper most edge piezometer P2 and the uppermost centreline piezometer P4. The failure plane is believed to be near to piezometer P2 based on inclinometer measurements.

Lateral movements increased gradually with increase in embankment height but with distinctly greater rapidity after placement of the final lift. At the same time as the pore pressure at P2 registered a rapid increase under constant load the location of the maximum shear plane along the inclinometer dropped to R.L. -6.0m corresponding to the location of the critical failure surface from total stress analysis.

No single parameter could be used to determine the time and fill height when instability would take place. All parameters tended to indicate increasing instability only after placement of the last layer of fill. However trends toward instability took place before appearance of tension cracks.

A more deterministic approach would be to carry out "a posteriori" type Effective Stress Analysis as reported in Section 7.1 of this paper and shown in Fig. 14.

7.2.2 SCHEME 6/2

Fig. 16 illustrates plots of fill thickness, pore pressures, lateral movements and the locations of the maximum simple shear strain with time.

A distinctly faster rate of lateral movement increase occurred immediately after placement of the final lift followed a few days later by a drop in the location of the maximum shear along the inclinometer to R.L. -6.2m, all these taking place before appearance of tension cracks.

Pore water pressures along the edge piezometers P1 and P2 recorded an increase of pore water pressure while pore pressure reduction occurred at the centreline piezometers P4 and P5. At failure, piezometer P2 (near to the failure plane) showed higher excess pore pressures than piezometer P4.

It is of interest to note that the pore pressure decrease at P4 may be indicative of local unloading due to stress redistribution within the continuum as a result of work softening. The model shown in Fig. 17 serves to explain this behaviour.

Application of a vertical compressive stress across the rigid platens results in increases in the compressive stresses in springs A, B and C. Supposing an increased load ΔP is applied and spring A work softens resulting in increased rate of pore pressure buildup, the reactions on springs B will decrease i.e. unload elastically with a decrease in pore water pressure, and the work released by spring A plus the increased external load will be absorbed by springs C.

It should be noted that such pore pressure decrease at P4 did not occur at Scheme 6/1. It is evisaged such behaviour as described by the model may have taken place at Scheme 6/1 but that the location of P4 did not coincide with zones of elastic unloading.

7.2.3 SCHEME 3/5

The plots of fill thickness, pore pressures, lateral movements and location of the maximum shear strain are given in Fig. 18. As distinct from Schemes 6/1 and 6/2 the embankment was raised at a near constant rate.

Except for piezometer P8A all piezometers shown increases with increasing fill thicknesses.

Embankment failure occurred at a fill thickness of about 5.4m.

A significant rate of increase of lateral movements commenced at the time when the location of the maximum shear plane dropped to R.L. -5.8m. This occurred at an embankment fill thickness of 4.8m, the thickness at which Scheme 6/1 failed. This implies the possibility that if the embankment fill had been maintained at a thickness of 4.8m, failure of the embankment might well have occurred after some time.

As for the previous two embankments, the reduction in the R.L. of the maximum shear plane to R.L. of -5.8m for the toe inclinometer occurred before tension cracks were reported.

Fig. 14 illustrating the Factor of Safety with time for Scheme 3/5 showed a sudden drop in the Factor of Safety when the maximum shear plane adjusted to the levels corresponding to the failure plane. However the Factor of Safety computed by "a posteriori" types of Effective Stress Analysis was 1.06. This may be due to the method of estimating the actual pore pressures across the failure plane viz linear interpolation of pore pressures at piezometers, adopted in the analysis. Nonetheless the use of this type of analysis together with an overall study of the different parameters still forms the best approach to monitoring the stability of an embankment during construction.

8.0 EMBANKMENTS THAT UNDERWENT SIGNIFICANT LATERAL MOVEMENTS BUT REMAINED STABLE

Notwithstanding the evidence to suggest that instability can be predicted by the parameters described in Section 7.0, Schemes 3/3 and 3/4 did not fail despite significant lateral movements and large tension cracks.

Figs. 19 and 20 are plots of fill thickness, pore pressures (Scheme 3/4 only), lateral movements and levels of the maximum shear strain. Unfortunately no piezometers were located at Scheme 3/3 at the designer's request.In both cases the rate of lateral movement reduced significantly after the stage of rapid filling was complete with the location of maximum shear occuring at between -5.0m and -6.0m.

In the case of Scheme 3/4 some reduction of pore pressure occurred at the centreline piezometer P4 while increase in pore pressures occurred for some of the other piezometers. It cannot be certain if this decrease in pore pressures is due to pore pressure dissipation or pore pressure redistribution of the nature described in the previous section.

In comparison Fig. 21 illustrates the different parameters for a stable embankment (Scheme 3/2) also built fairly rapidly. The lateral movements were not excessive and no tension cracks appear. Pore pressure dissipation was minimal and the level of the maximum shear plane remained at a relatively high level.

9.0 PILED EMBANKMENT

The piled embankment failed due to instability of the berms which were without piles.

Measurements from load cells (P_{pile}) are shown in Fig. 22. The percentage of the embankment load transferred to the pile is taken to be :-

$$(P_{pile}/P_{total}) \times 100$$

where P_{total} is the theoretical total weight of the embankment. As shown in Fig. 22 the percentage of the load transferred to the pile the ranges from 40 to 60%.

This is contrary to the design assumptions but consistent with longer term observations of similar pile embankments elsewhere where excessive settlements have occurred between pile caps.

10.0 CONCLUSIONS

A study of the instrumentation results shows that :-

(i) Dissipation of pore pressures is a very significant element of soil treatment;

(ii) Scheme 6/7 and possibly Scheme 6/5 were the only schemes able to attain a relatively high degree of consolidation. In the case of Schemes 6/7 this was undoubtedly due to the positive removal of water from the prefabricated vertical drains by the vacuum pump;

(iii) Pore pressure dissipation was observed to be directly related to gain in strength, degree of consolidation and lateral movements. Failure to dissipate pore water pressures were consistent with low gain in strengths which were in any case limited to near the drainage blankets, low degree of consolidation settlements and relatively higher amounts of lateral movements;

(iv) All schemes show volumetric change during embankment filling and undrained conditions do not exist, except just prior to failure. Volume changes corresponding to a Poisson's ratio of 0.3 were consistant with excessive lateral movements and tension cracks. Volumetric changes for the more stable embankments indicate Poisson's ratio of much less than 0.3.

11.0 REFERENCES

1. Chee, S.K. (1991)

   "Embankments on Malaysian Marine Clays - A Case Study of Instability." First Young Geotechnical Engineers Conference, Bangkok.

2. Giroud, J.P. (1973)

   Tables pour le calcul dec fondations. Dunod, Paris.

3. Leroueil, S. and Tavenas, F. (1986)

   Discussions. Canadian Geotech. Jnl. Vol 23, pp 410 to 413.

4. Shibata, T. (1987)

   "Lateral Deformations of Clay Foundations" Discussion Session 6. Proc. 8th Asian Regional Conf. on S.M.F.E. Kyoto, Vol. 2, pp 390 to 391.

5. Tavenas, F. and Leroueil, S. (1980)

   "The Behaviour of Embankments on Clay Foundations".
   Can. Geotech. Jnl. Vol. 17, pp 236 to 260.

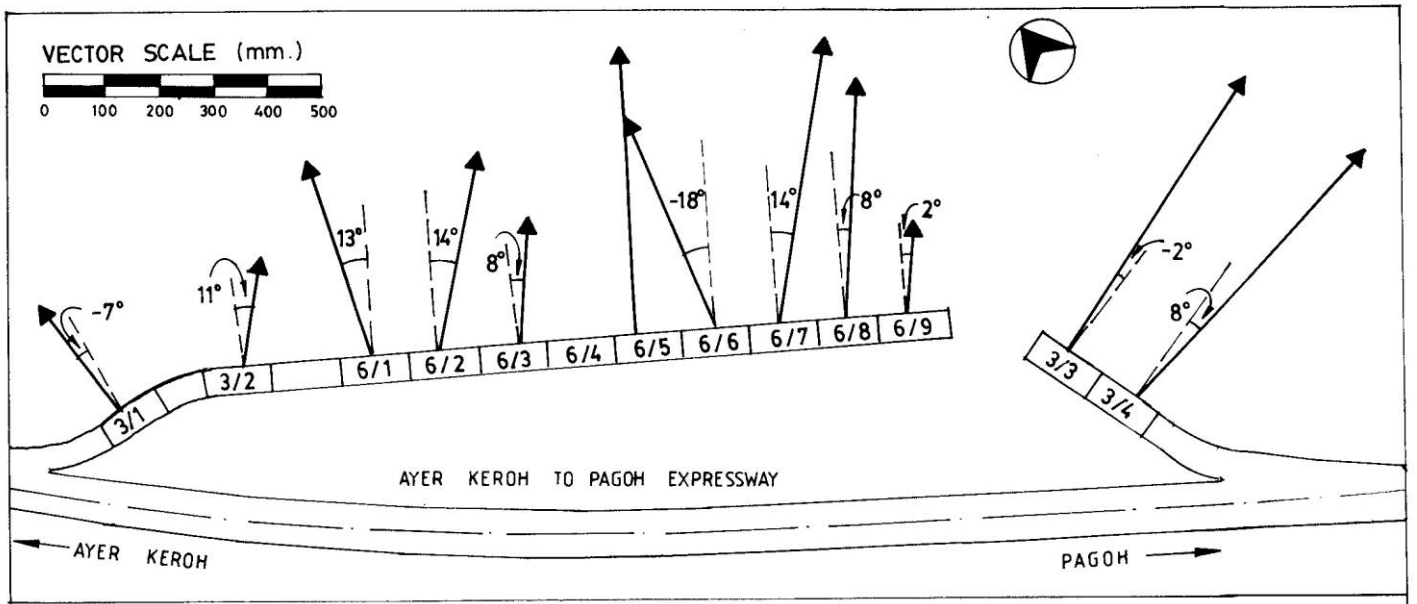

Fig. 1 MOVEMENT VECTORS AT R.L 0·00m (-2·4m depth)

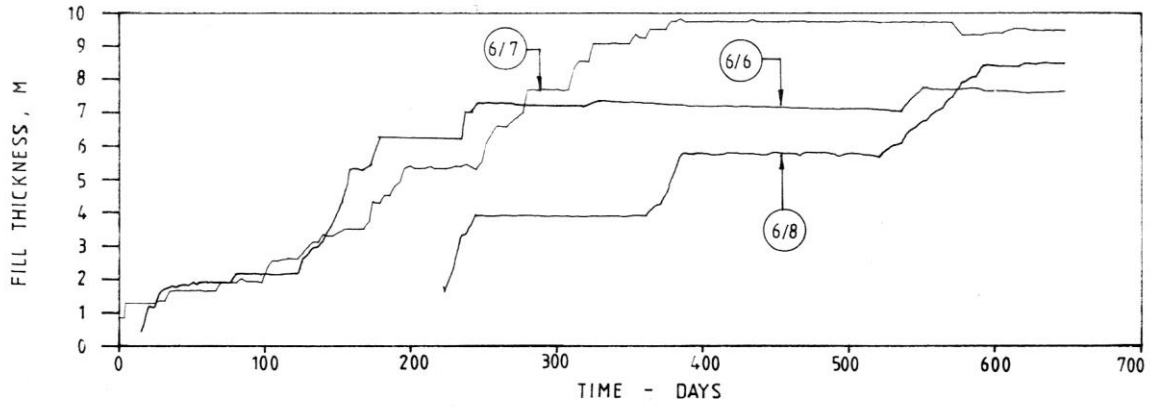

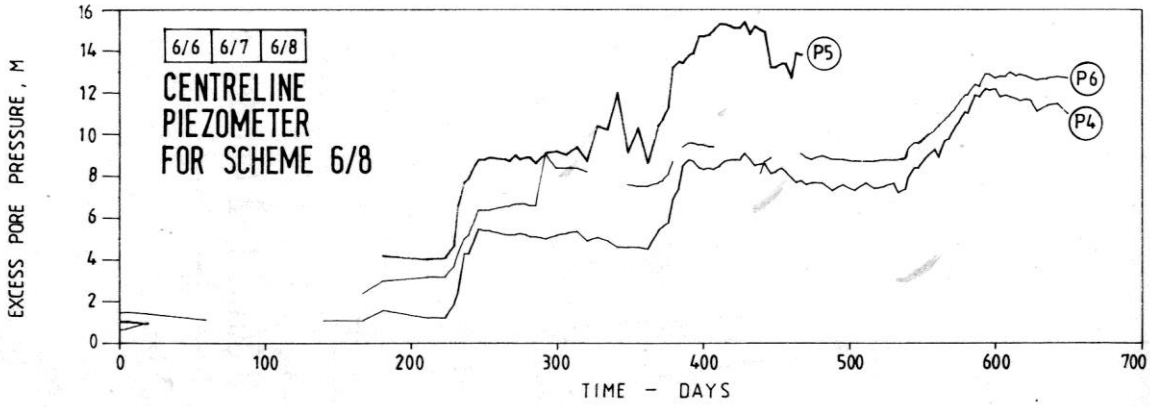

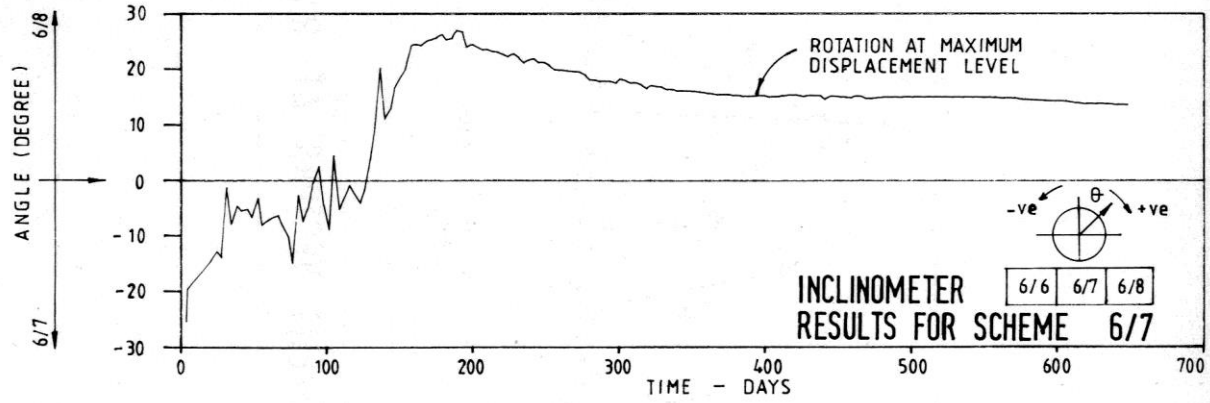

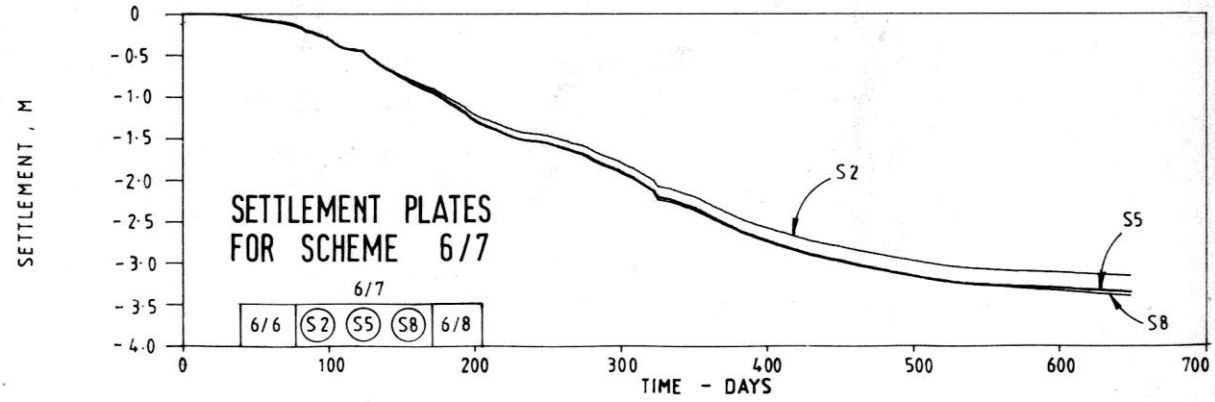

Fig. 2 "INTERFERENCE" BETWEEN SCHEMES

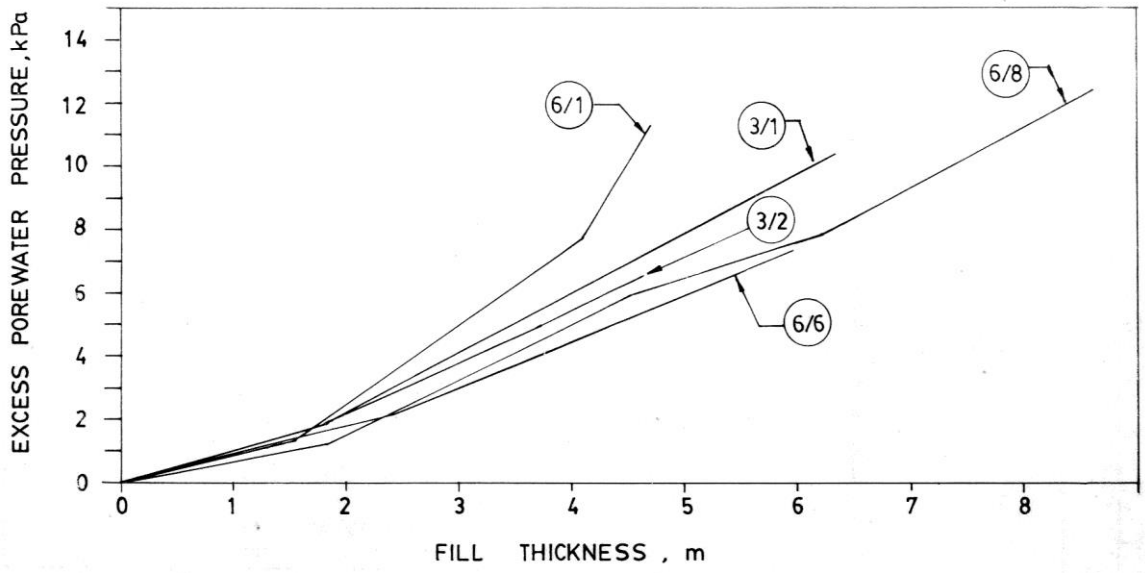

Fig. 3 EXCESS PORE WATER PRESSURE RESPONSE

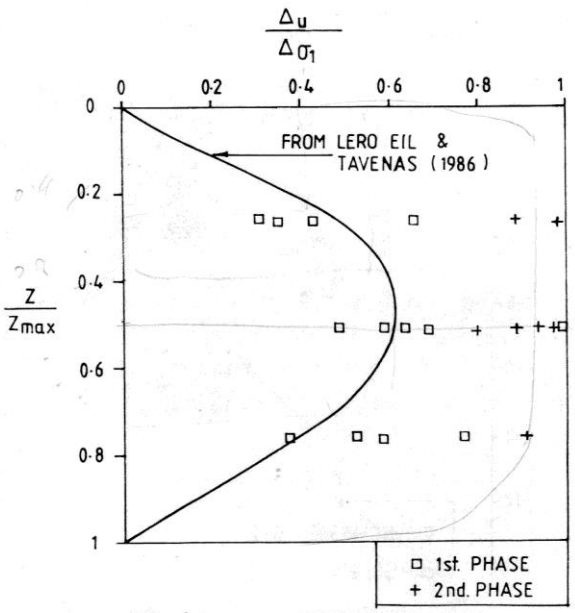

Fig. 4a CENTRELINE PIEZOMETER

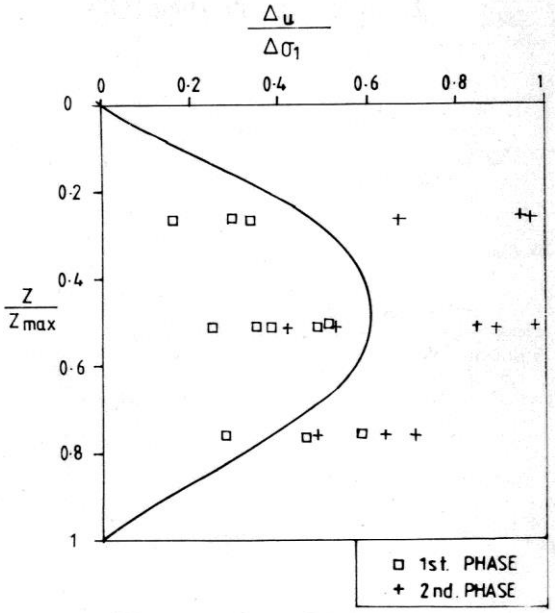

Fig. 4b EDGE PIEZOMETER

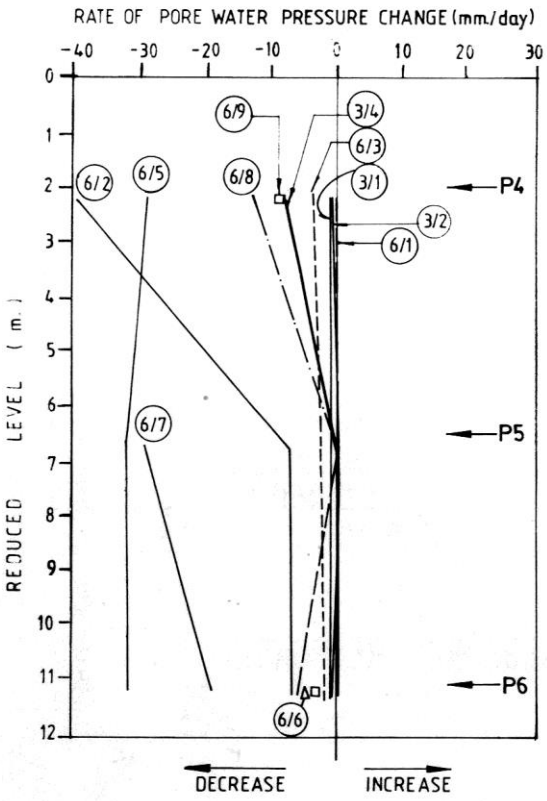

Fig. 5 RATES OF CHANGES OF PORE WATER PRESSURE (CENTRELINE PIEZOMETERS)

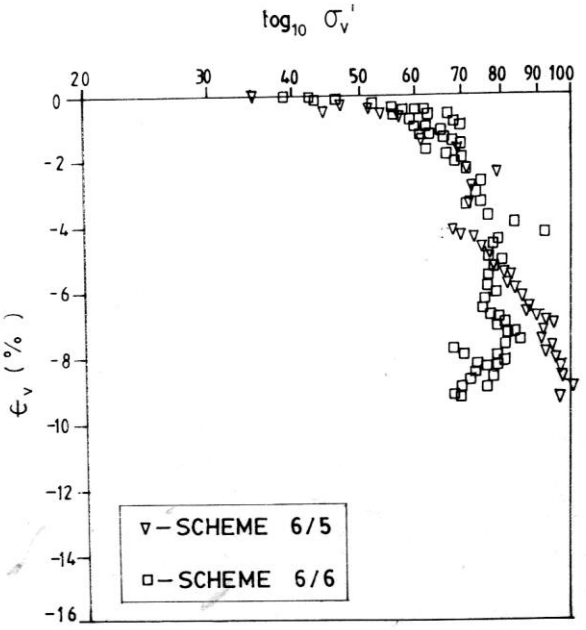

Fig. 6a FIELD ϵ_v - $\log_{10} \sigma_v'$ (PIEZOMETER P4)

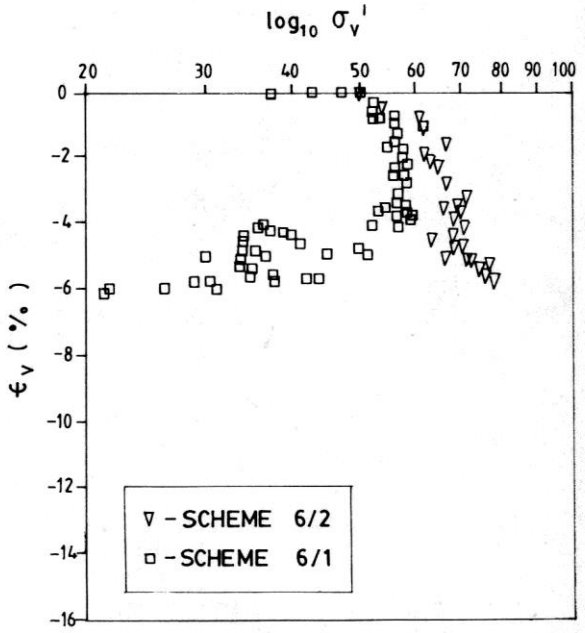

Fig. 6b FIELD ϵ_v - $\log_{10} \sigma_v'$ (PIEZOMETER P4)

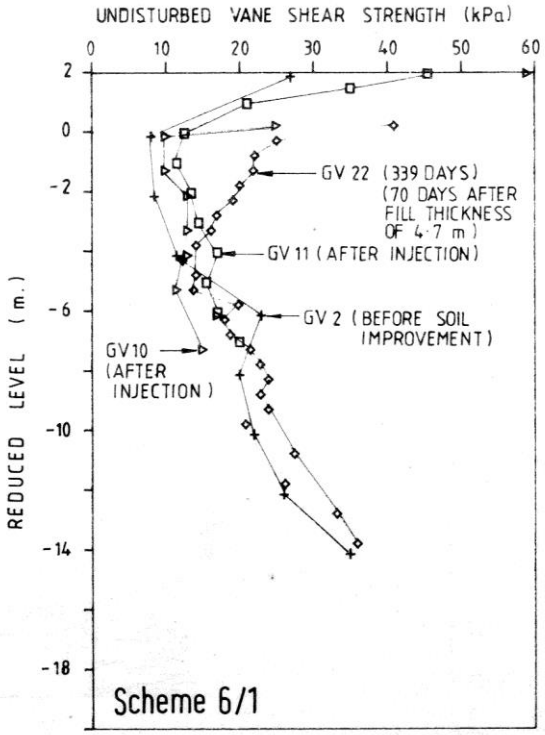

Fig. 7a GAIN IN STRENGTH

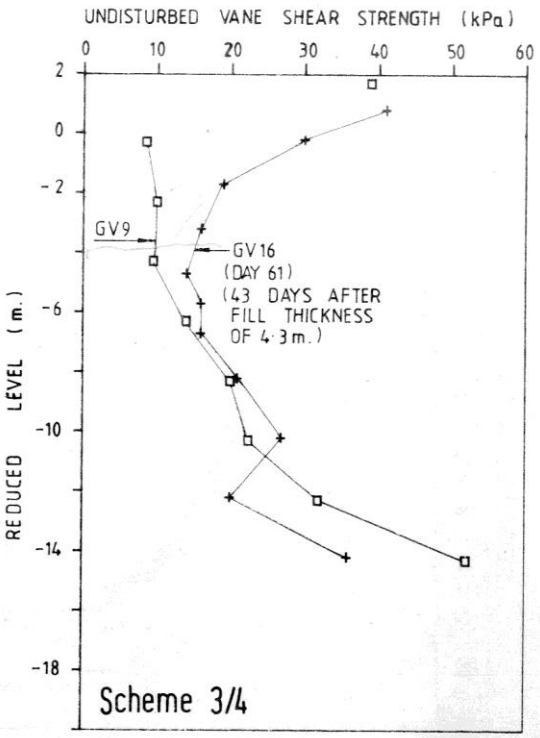

Fig. 7b GAIN IN STRENGTH

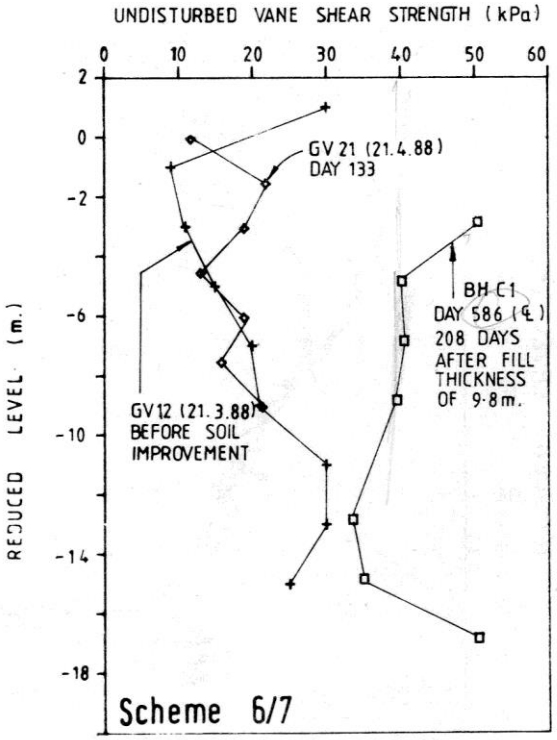

Fig. 7c GAIN IN STRENGTH

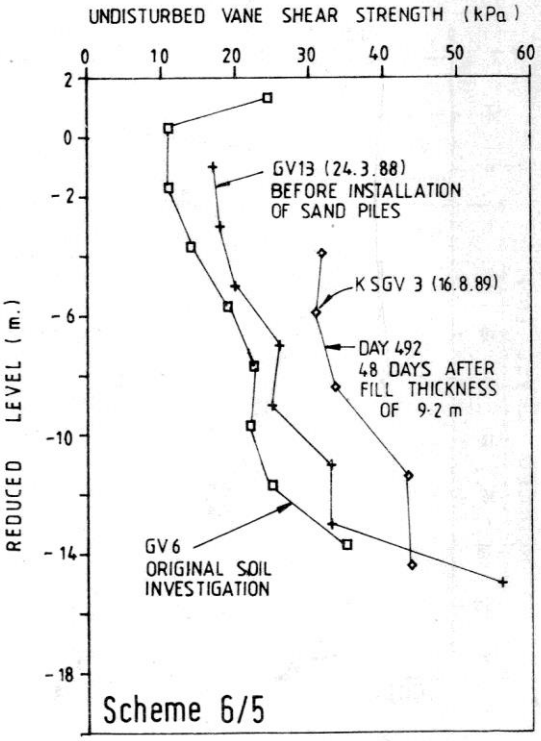

Fig. 7d GAIN IN STRENGTH

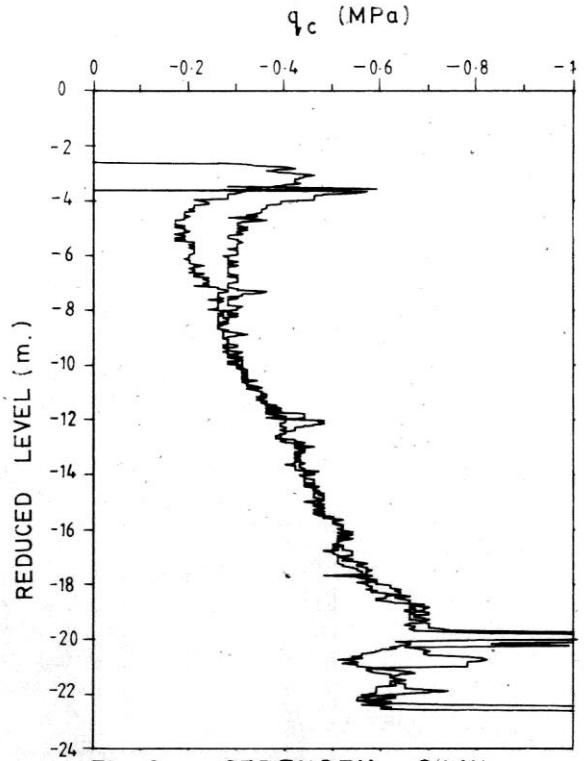

Fig. 8a STRENGTH GAIN PROFILE - SCHEME 3/2

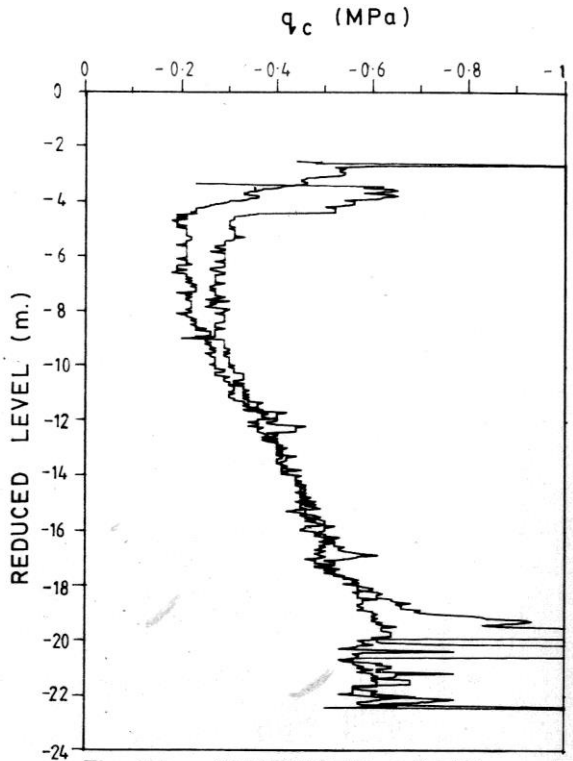

Fig. 8b STRENGTH GAIN PROFILE - SCHEME 3/1

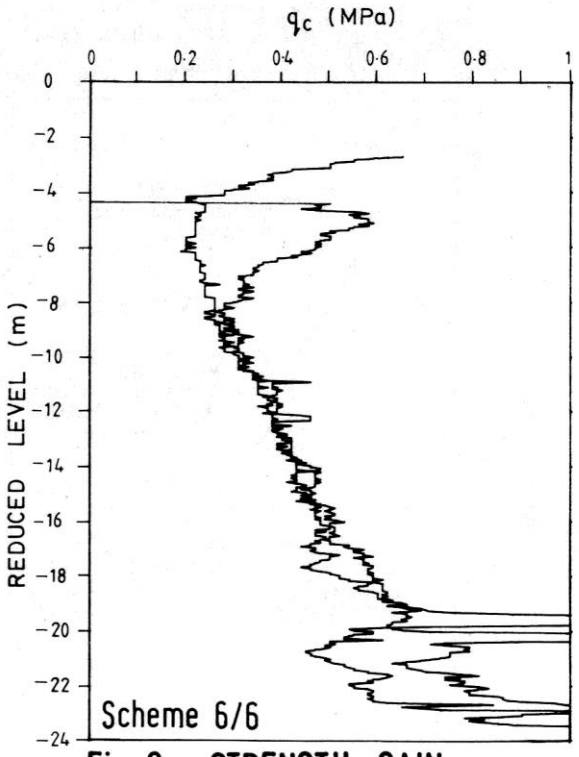

Fig. 8c STRENGTH GAIN PROFILE - SCHEME 6/6

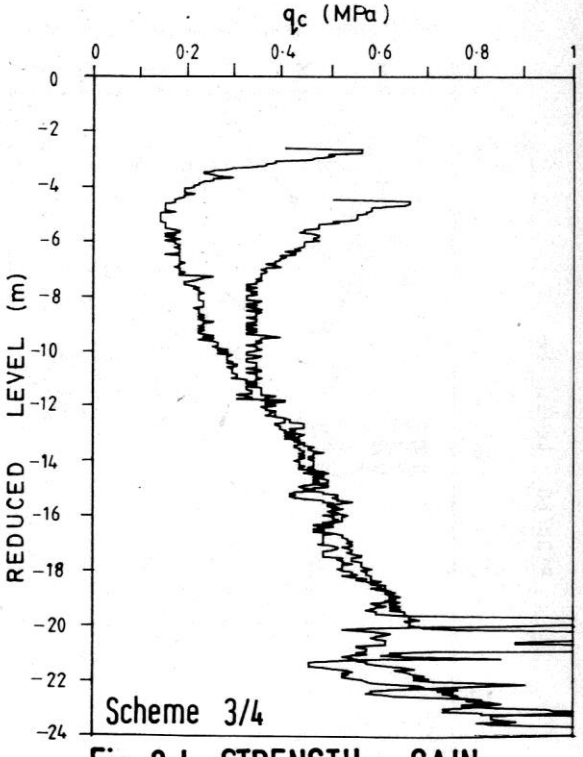

Fig. 8d STRENGTH GAIN PROFILE - SCHEME 3/4

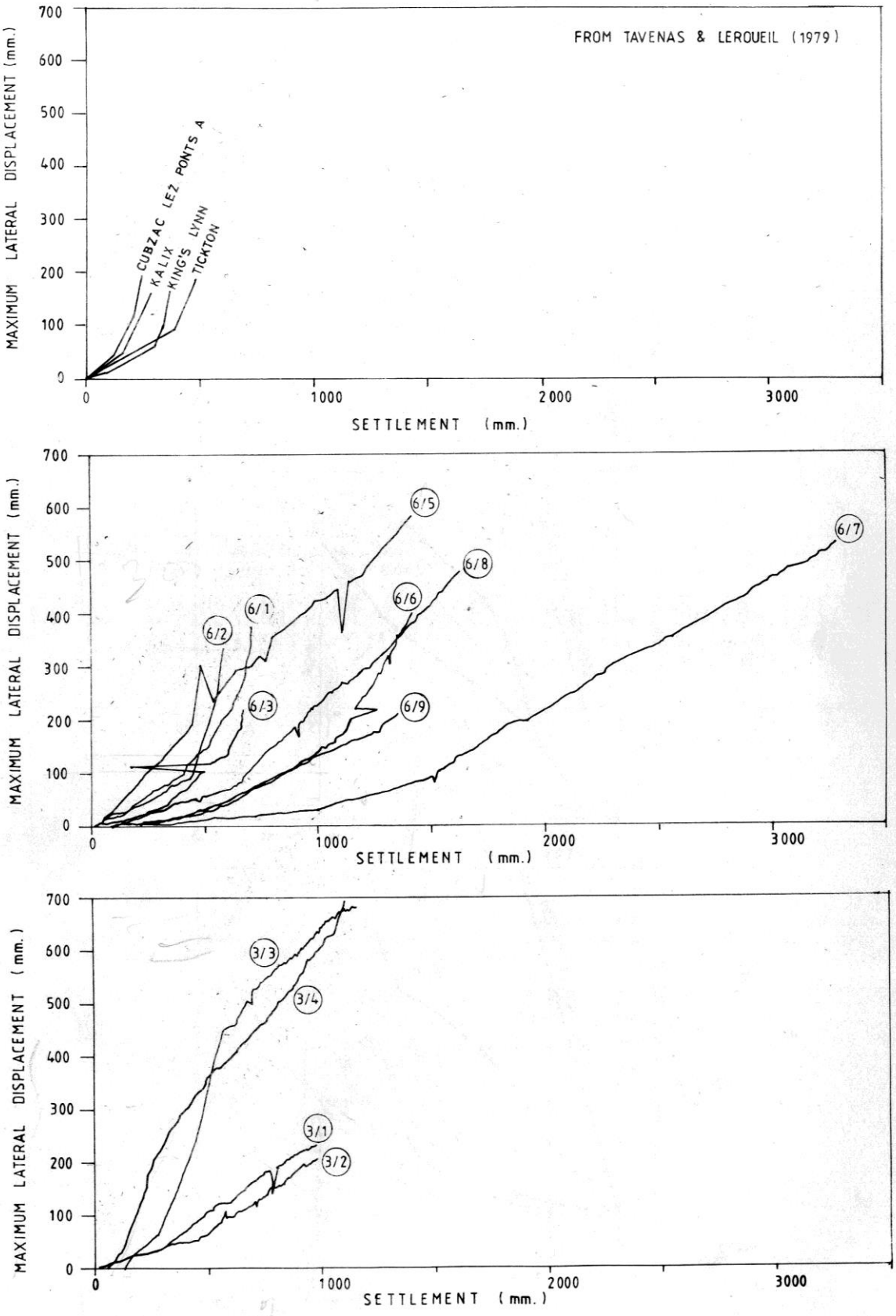

Fig. 9 LATERAL DISPLACEMENT - VERTICAL SETTLEMENT

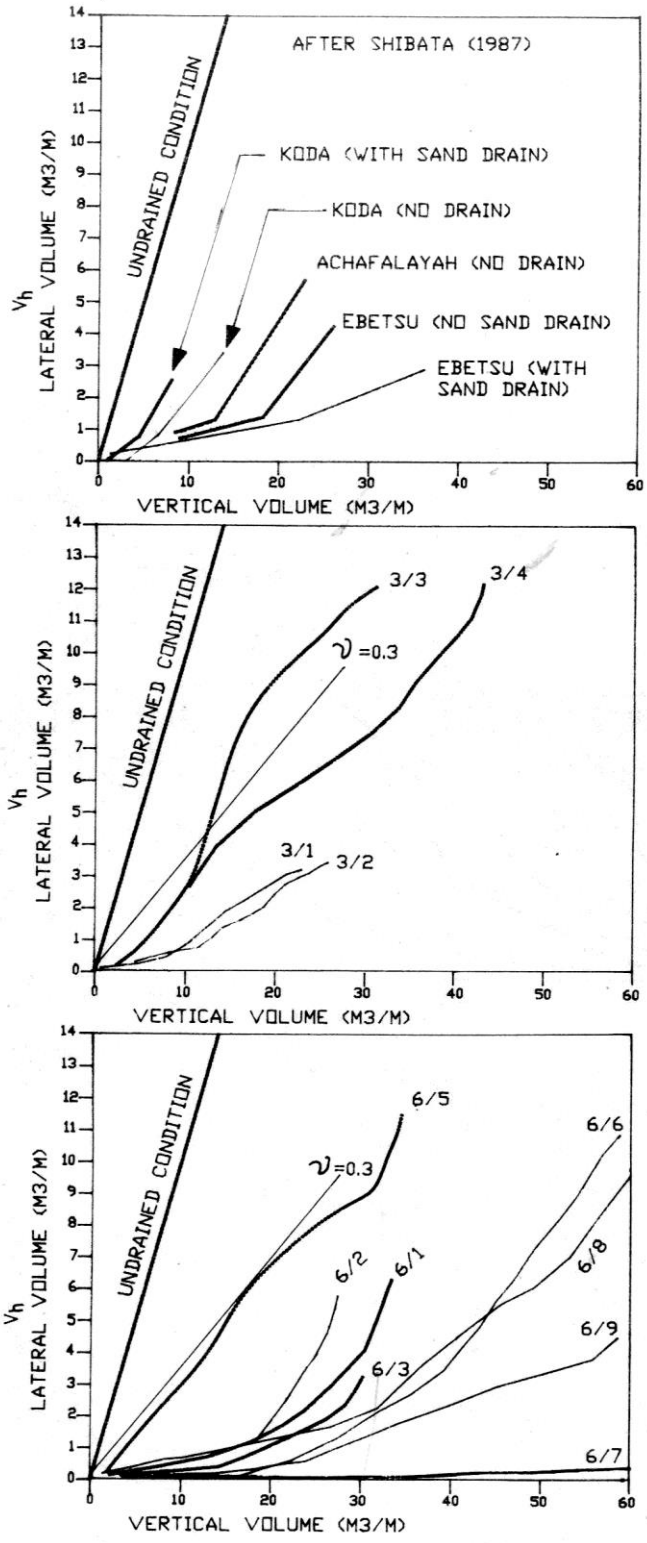

Fig. 10. LATERAL - VERTICAL VOL.

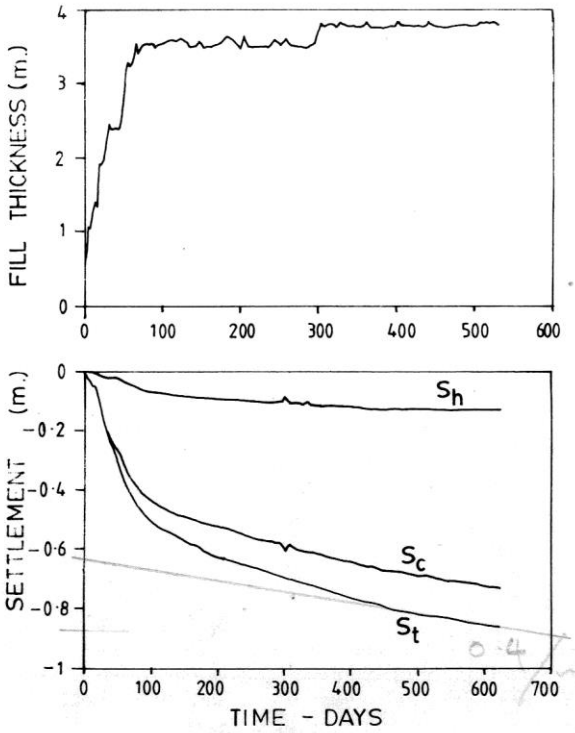

Fig. 11a COMPONENTS OF SETTLEMENT - 3/1

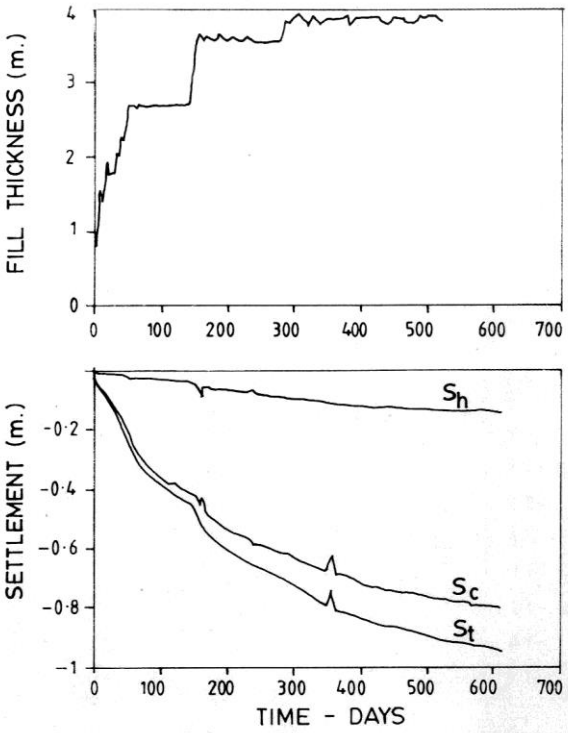

Fig. 11b COMPONENTS OF OF SETTLEMENT - 3/2

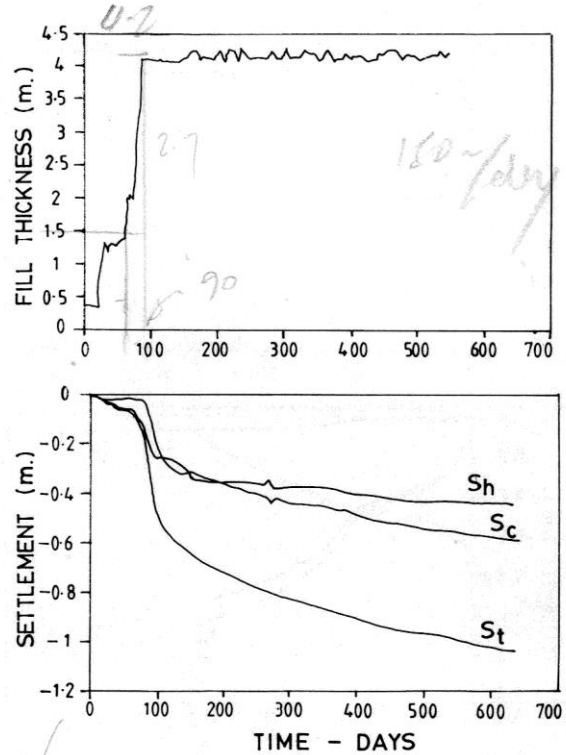

Fig. 11c. COMPONENTS OF SETTLEMENT - 3/3

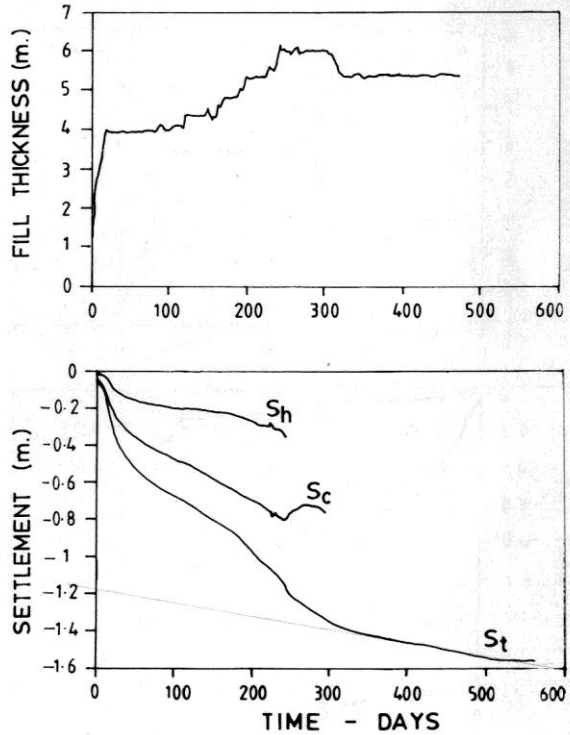

Fig. 11d. COMPONENTS OF SETTLEMENT - 3/4

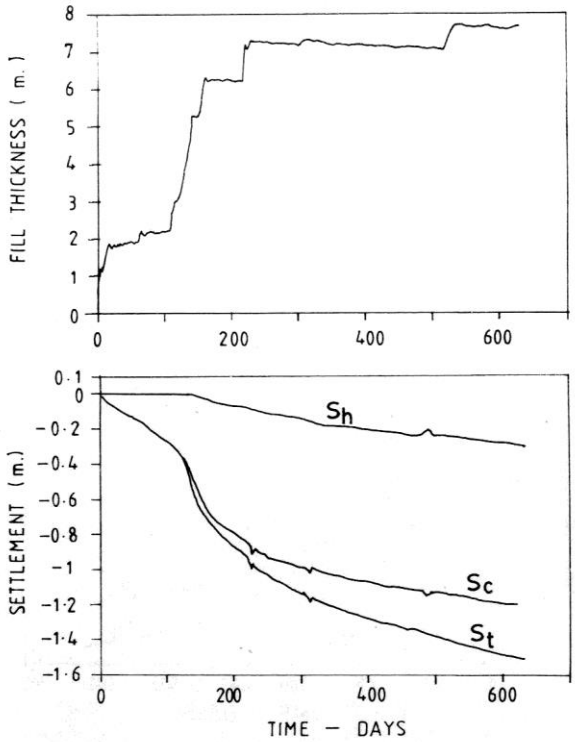

Fig. 11e COMPONENTS OF SETTLEMENT – 6/6

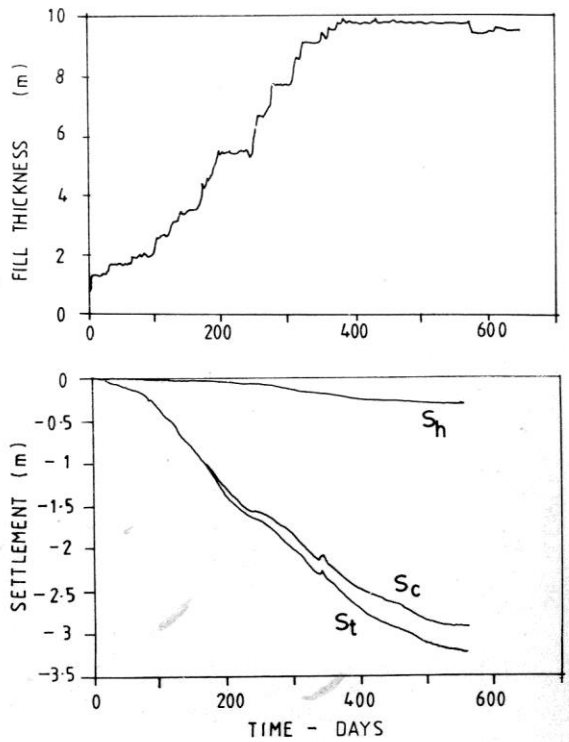

Fig. 11f COMPONENTS OF SETTLEMENTS – 6/7

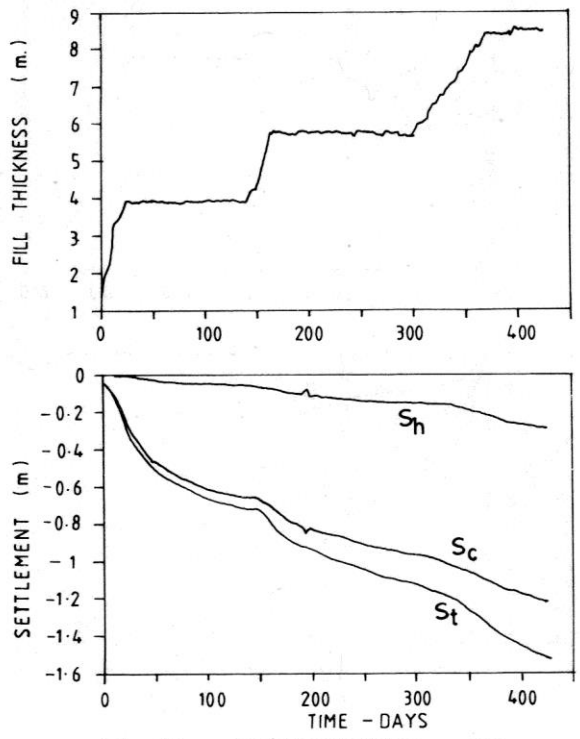

Fig. 11g COMPONENTS OF SETTLEMENTS – 6/8

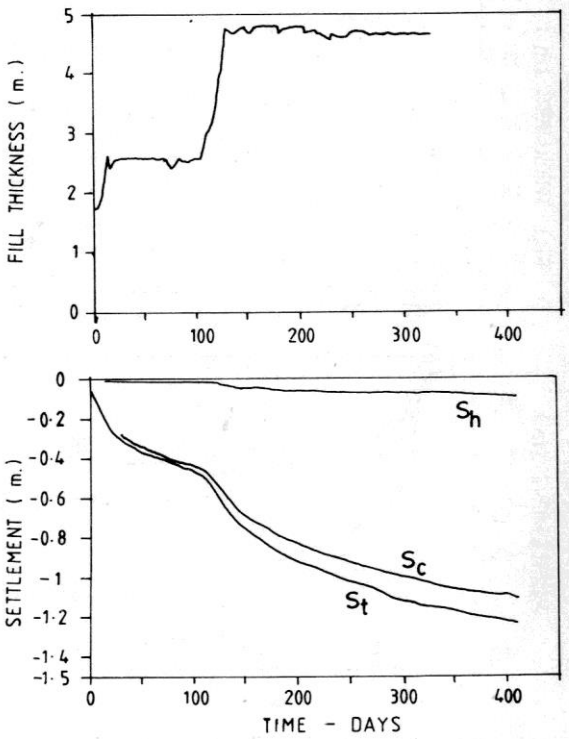

Fig. 11h COMPONENTS OF SETTLEMENTS – 6/9

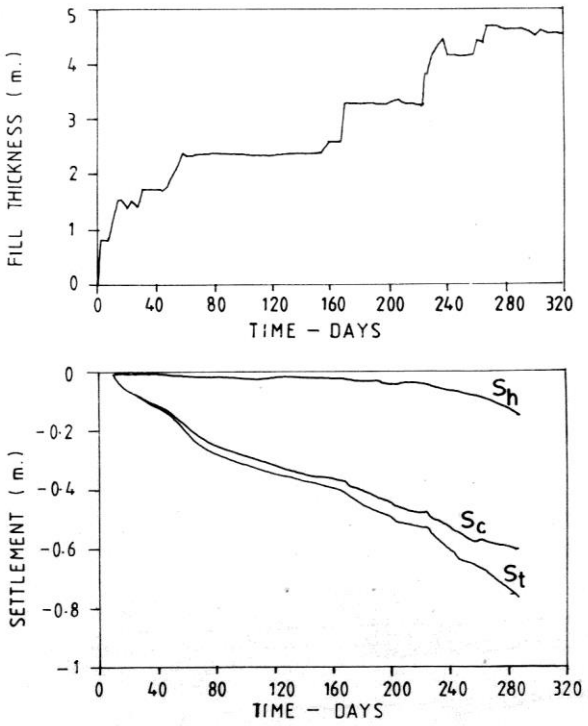

Fig. 11i COMPONENTS OF SETTLEMENT - 6/1

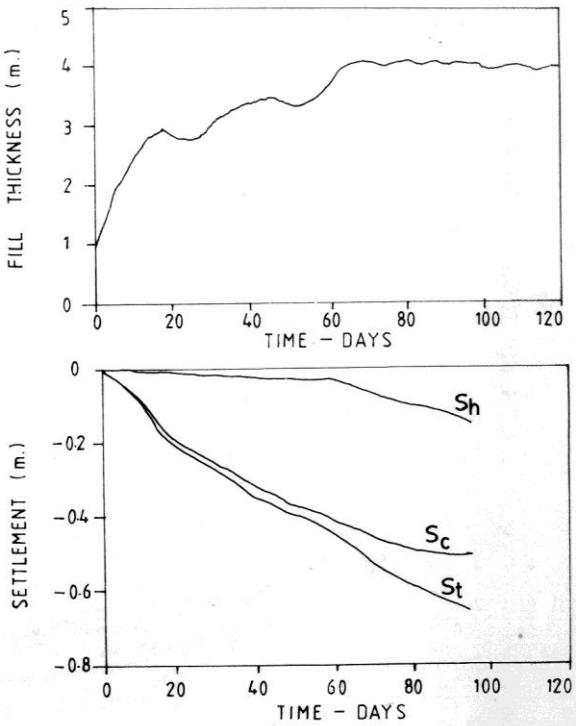

Fig. 11j COMPONENTS OF SETTLEMENT - 6/2

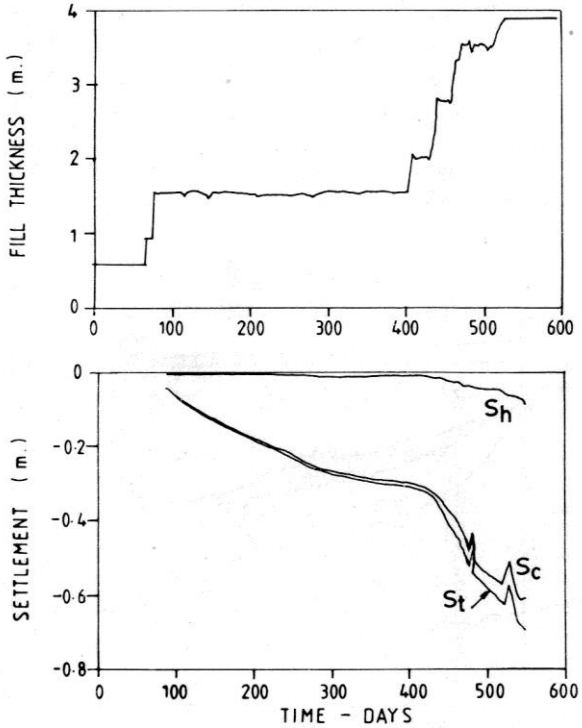

Fig. 11k COMPONENTS OF SETTLEMENT - 6/3

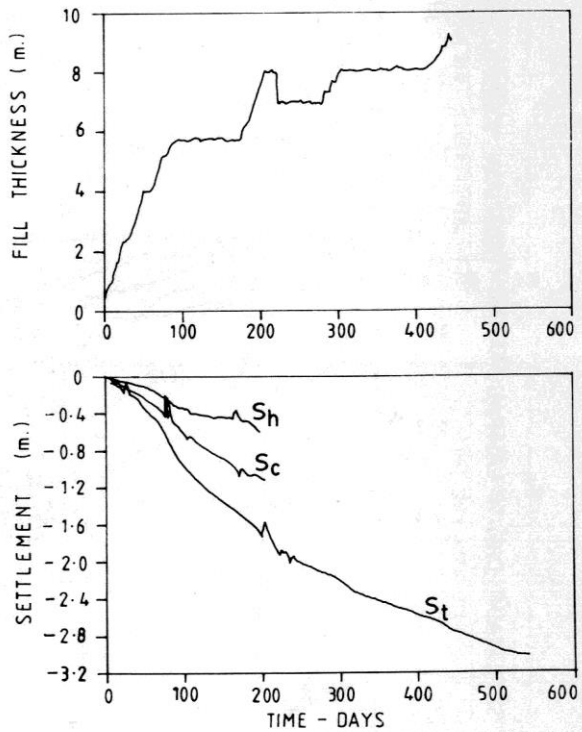

Fig. 11l COMPONENTS OF SETTLEMENT - 6/5

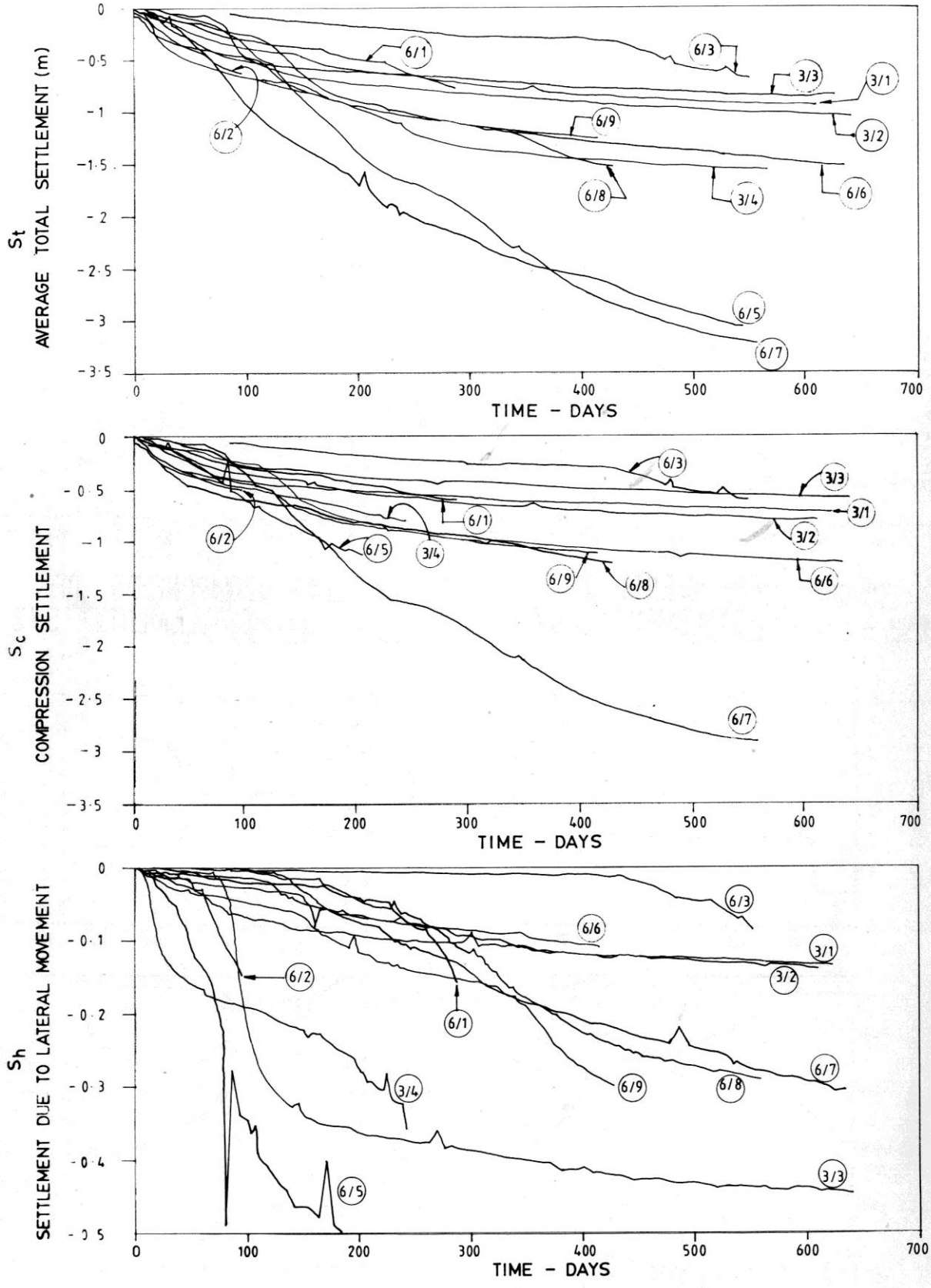

Fig. 12 COMPARISON OF COMPONENTS OF SETTLEMENT

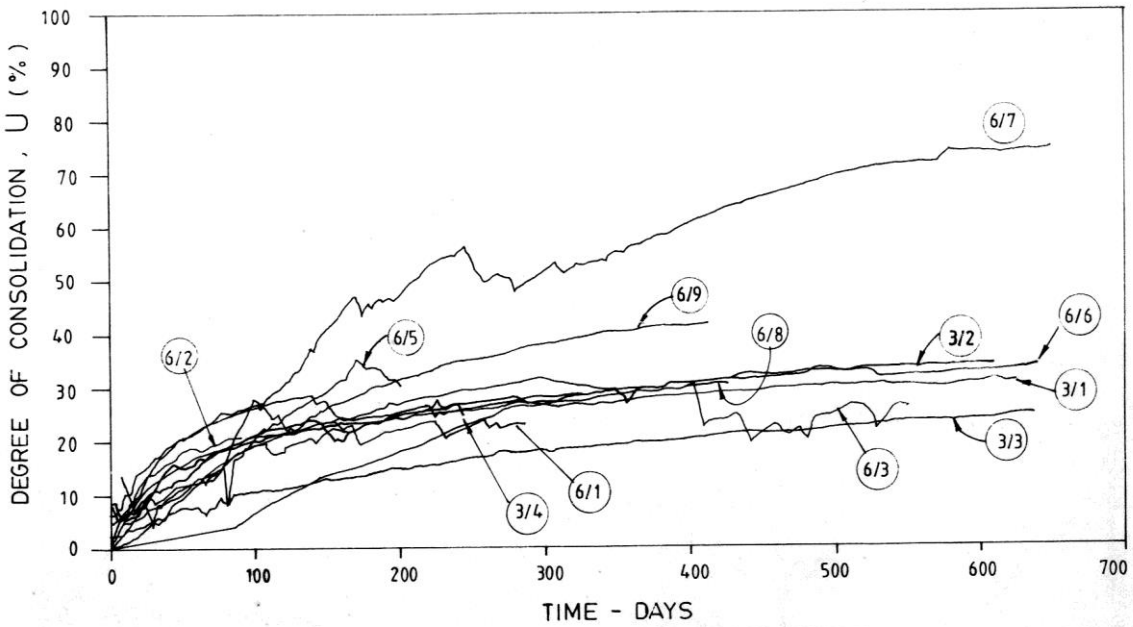

Fig. 13. DEGREE OF CONSOLIDATION

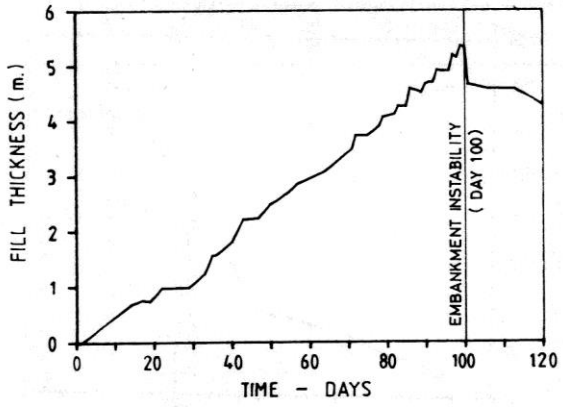

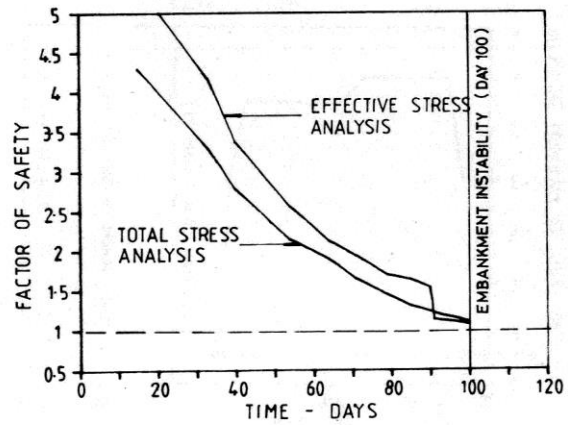

Fig. 14a. SCHEME 3/5

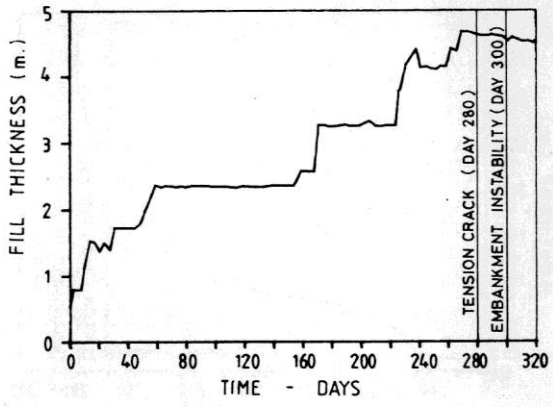

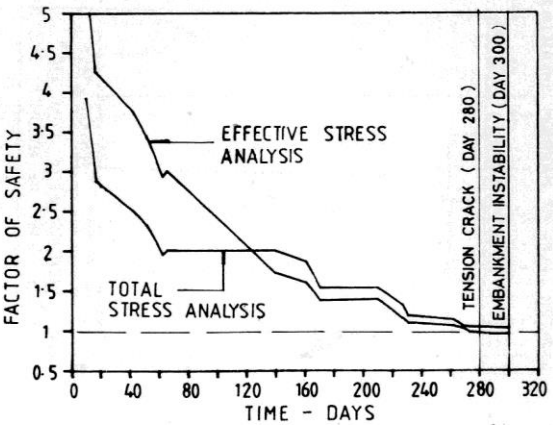

Fig. 14b SCHEME 6/1

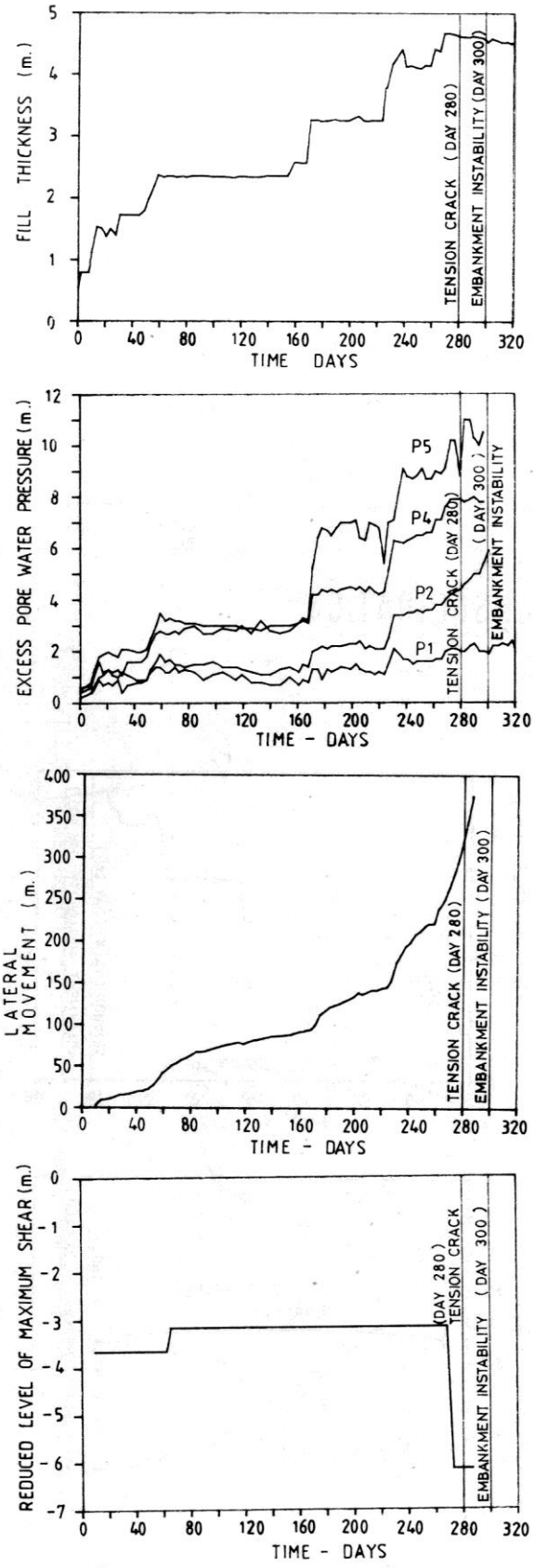

Fig. 15 SCHEME 6/1

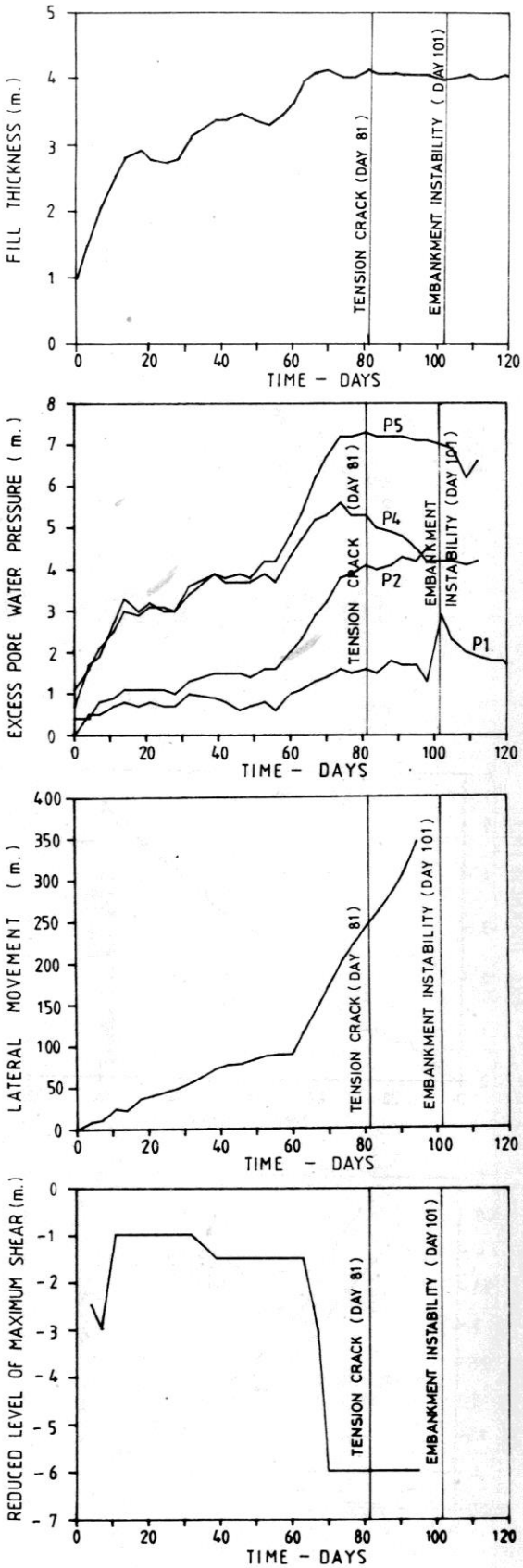

Fig. 16 SCHEME 6/2

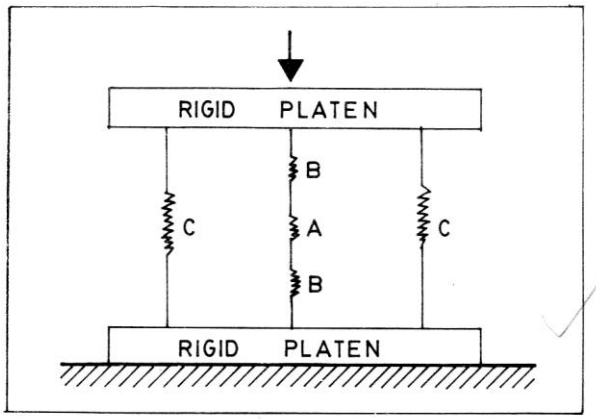

Fig. 17 SPRING MODEL

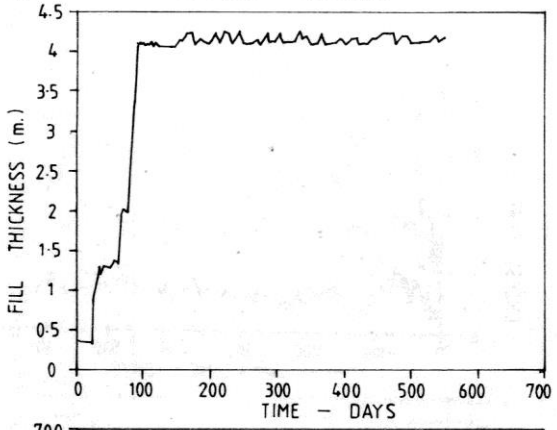

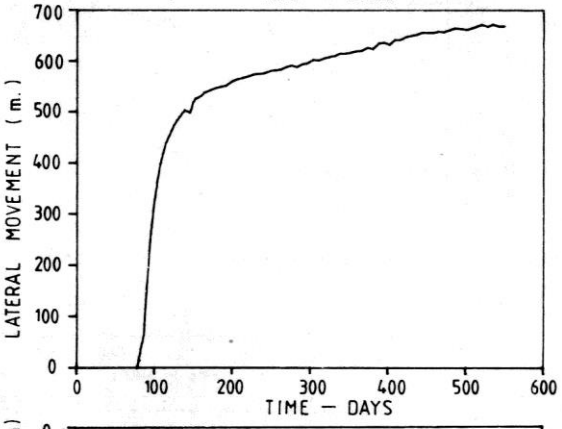

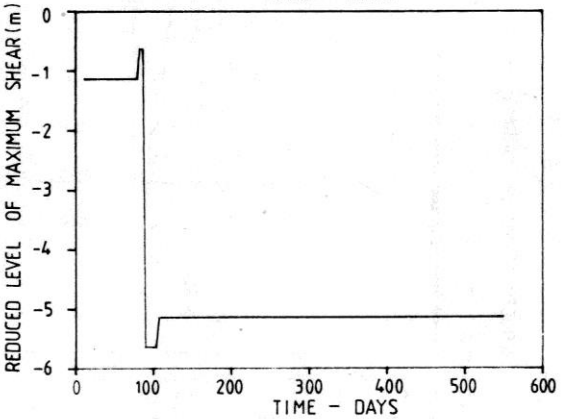

Fig. 19 SCHEME 3/3 [600 DAYS]

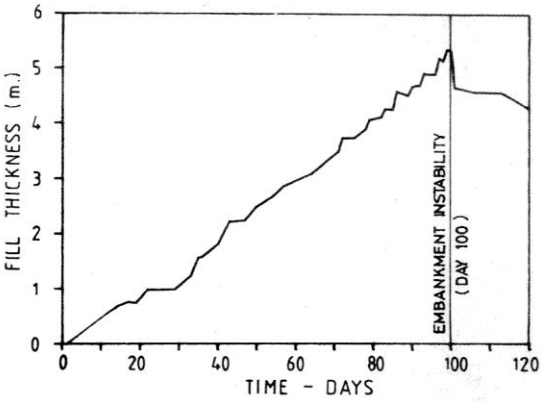

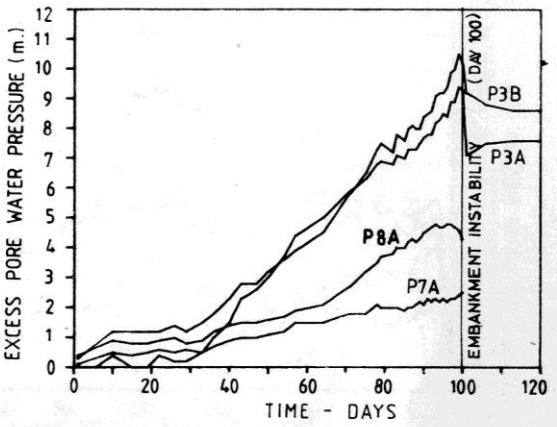

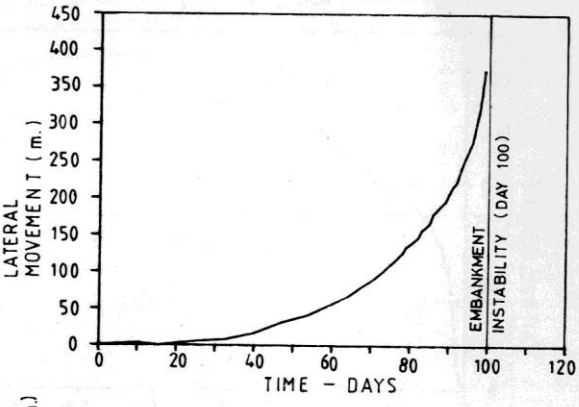

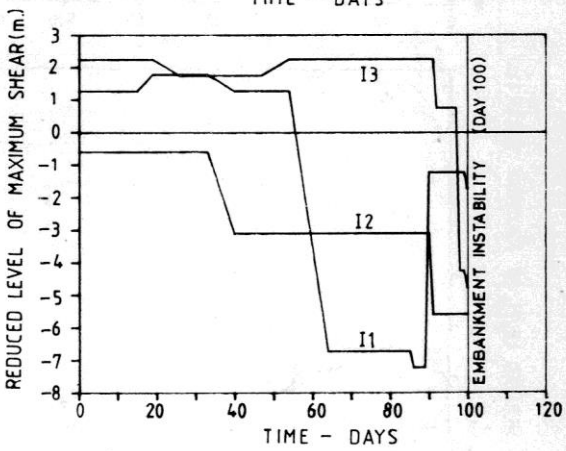

Fig. 18 SCHEME 3/5

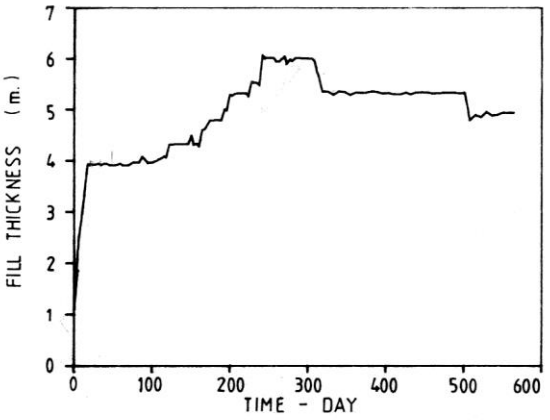

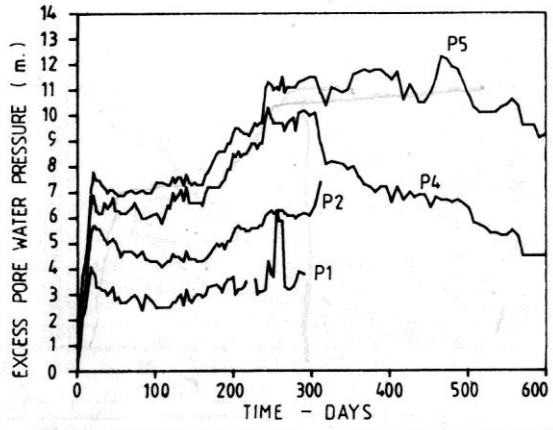

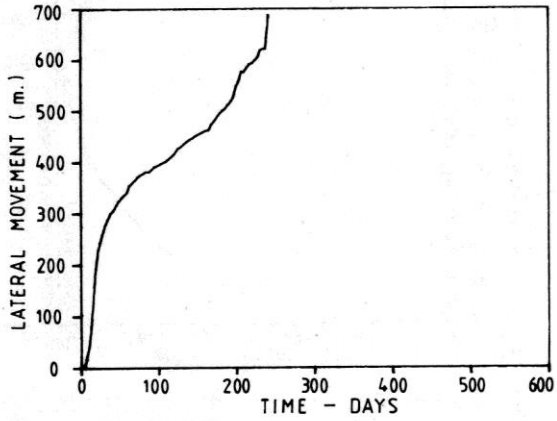

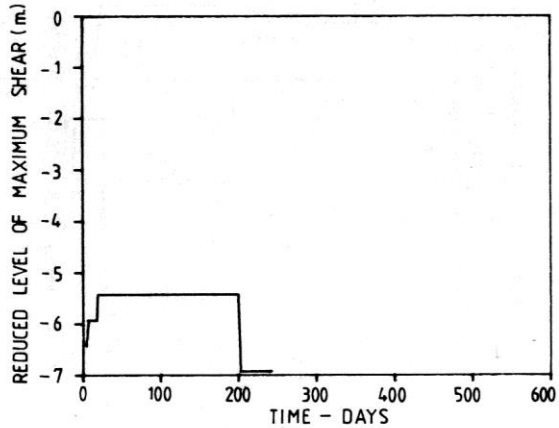

Fig. 20 SCHEME 3/4

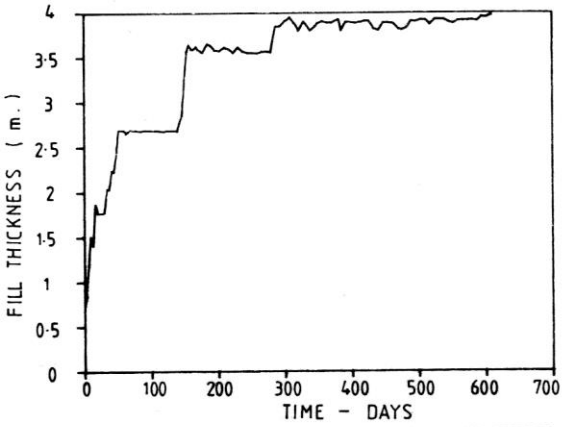

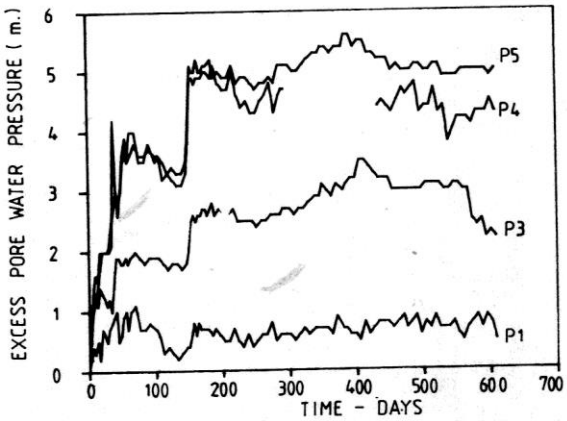

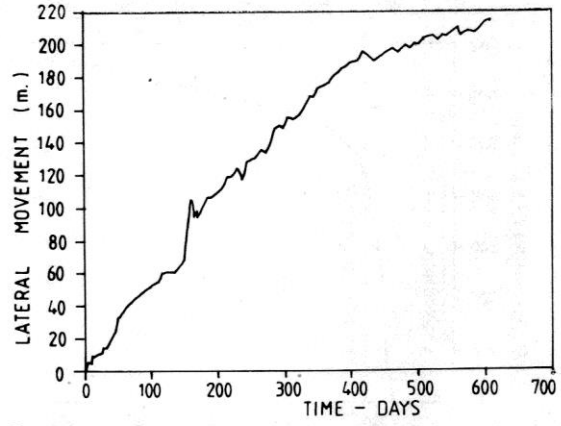

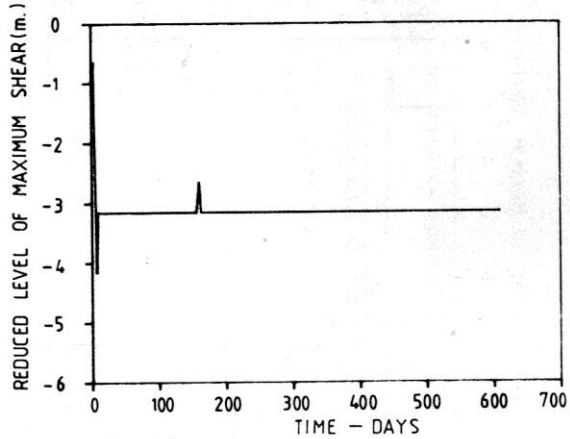

Fig. 21 SCHEME 3/2

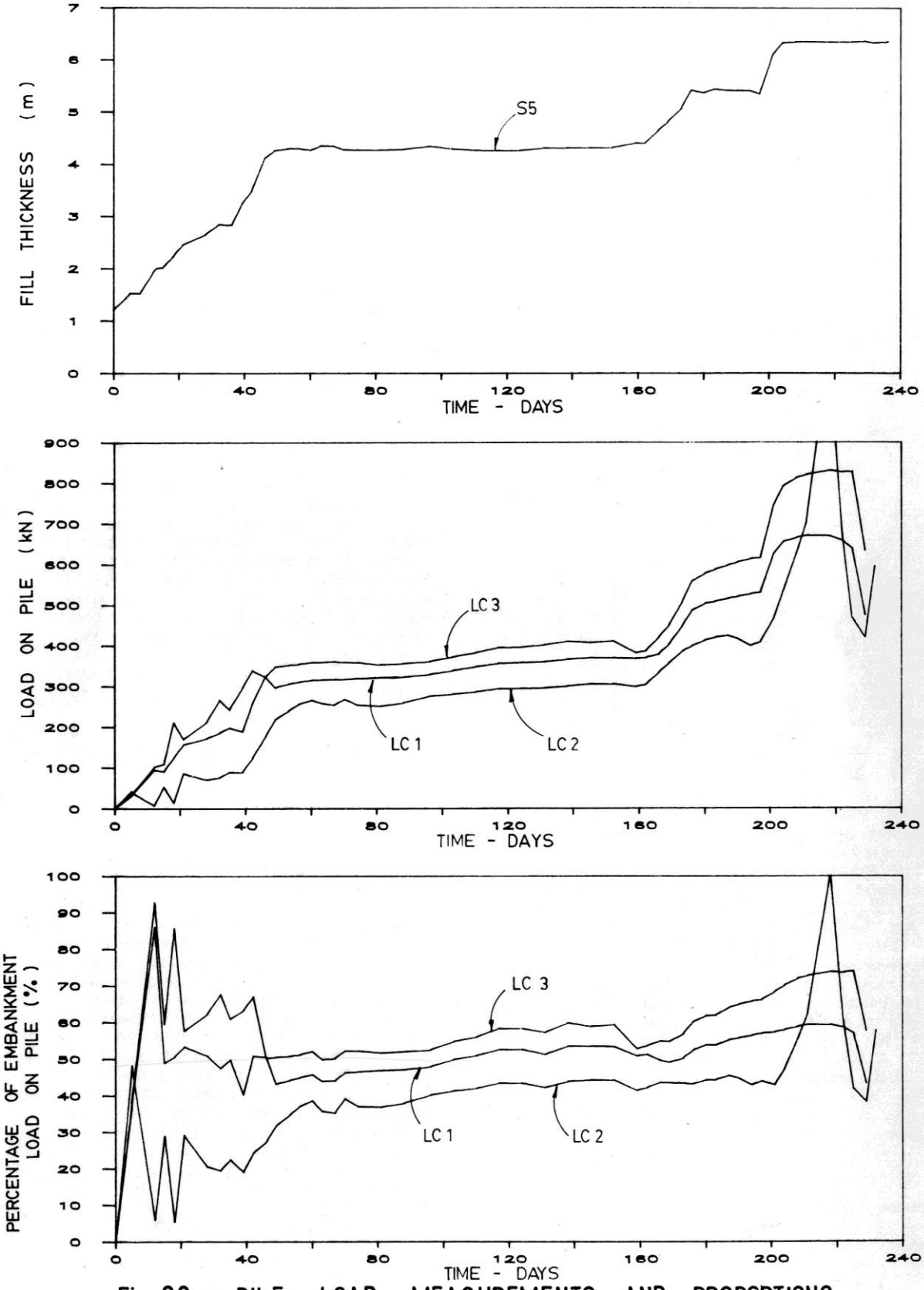

Fig. 22 PILE LOAD MEASUREMENTS AND PROPORTIONS OF LOAD TRANSMITTED TO PILES